Materials Science and Engineering A 372 (2004) 115–122

www.elsevier.com/locate/msea

The microstructure of mechanically alloyed Al–Mg determined by X-ray diffraction peak profile analysis

J. Gubicza [a,b], M. Kassem [c], G. Ribárik [b], T. Ungár [b,*]

[a] *Department of Solid State Physics, Eötvös University, P.O. Box 32, H-1518 Budapest, Hungary*
[b] *Department of General Physics, Eötvös University, P.O. Box 32, H-1518 Budapest, Hungary*
[c] *Department of Materials Science and Engineering, Faculty of Petroleum and Mining, Suez Canal University, Suez, Egypt*

Received 16 January 2003; received in revised form 22 October 2003

Abstract

The effect of the nominal Mg content and the milling time on the microstructure and the hardness of mechanically alloyed Al-rich Al–Mg solid solutions is studied. The crystallite size distribution and the dislocation structure are characterized by X-ray diffraction (XRD) peak profile analysis and the hardness is obtained from depth-sensing indentation tests. Magnesium gradually goes into solid solution during ball milling and after 3 h an almost complete solid solution is attained. With increasing milling time, the Mg concentration in solid solution, the dislocation density and the hardness increase, whereas the crystallite size decreases. A similar tendency of these parameters is observed at a particular duration of ball milling with increasing nominal Mg content. After 3 h milling there are no changes in both the microstructure and the hardness.

Keywords: Al–Mg alloys; Mechanical alloying; X-ray diffraction peak profile analysis; Crystallite size; Dislocation structure; Hardness

1. Introduction

Mechanical alloying (MA) is an effective tool to produce metallic alloys with fine microstructure. During the process the initial powder particles are deformed heavily and repeatedly by high energy milling and the atoms of the additions are soluted into the matrix of the main component. Ball milling is employed to obtain alloys with extended solubilities, dispersion-hardened metals, nanocrystalline and amorphous materials [1,2]. The ball milling-induced amorphization requires very high ball-to-powder ratio and moderate rotation speed since the friction and the sliding between the outer balls and the inner wall of the vial are the major events in amorphization [2]. At the same time in the production of crystalline alloys by MA the main mechanisms are the impact and the collision between the balls and the powder. During ball milling two essential processes occur—cold welding between the different particles and fracturing of the cold welded particles due to high energy collision [1]. The cold welding minimizes the diffusion distance between the atoms of the different components. The fracturing of the welded particles impedes the clustering of the particles promoting the transfer of the high ball collision energy to all particles and produces new, clean surfaces without oxide layers accelerating the diffusion [1].

X-ray diffraction (XRD) is often used for the characterisation of microstructure of crystalline materials. X-ray diffraction peak profiles are broadened, especially when crystallite size is lower than about 1 μm and/or the crystallites are distorted by lattice defects. The two effects can be separated on the basis of the different diffraction order dependence of peak broadening. The standard methods of X-ray diffraction profile analysis based on the full width at half-maximum (FWHM), the integral breadths and on the Fourier coefficients of the profiles provide the apparent crystallite size and the mean-square strain [3–6]. If the crystallites in a material can be assumed to have the same shape, a crystallite size distribution function having two free parameters can be also determined [7–12]. The evaluation of the X-ray profiles is complicated by the anisotropic strain broadening of the diffraction peaks [13–15]. This means that neither the full width at half maximum nor the integral breadth nor the Fourier coefficients of the profiles are monotonous functions of the diffraction vector. It has been shown that the strain anisotropy can be well accounted for by the dislocation

* Corresponding author. Tel.: +36-1-372-2801; fax: +36-1-372-2811.
E-mail address: ungar@ludens.elte.hu (T. Ungár).

0921-5093/$ – see front matter © 2004 Elsevier B.V. All rights reserved.
doi:10.1016/j.msea.2003.12.016

model of the mean-square strain by introducing the contrast factors of dislocations [16–21]. The contrast factors have been calculated for the most common cubic and hexagonal materials which can be used for the evaluation of diffraction profiles of dislocated crystals [22–25].

In the last few years considerable efforts have been made to develop procedures that can determine the parameters of the microstructure by fitting the whole diffraction profiles [26–31]. In the method proposed by Balzar size and strain broadened diffraction profiles are modelled by Voigt functions to obtain domain size and strain [26]. The correspondence between Cauchy and Gauss functions and the size and strain contributions to peak broadening, respectively, are discussed [26]. Scardi et al. [27] elaborated the so-called whole powder pattern fitting (WPPF) method in which the experimental profiles are fitted by Voigt functions and the characteristic parameters of these functions are related to the parameters of the microstructure. This method is developed further by introducing the whole powder pattern modelling (WPPM) procedure where the whole diffraction patterns are fitted by theoretical functions based on a microstructural model [28]. Ungár and co-workers [29,30] worked out the multiple whole profile (MWP) fitting method where the crystallite size distribution and the parameters of the dislocation structure are determined by fitting the measured physical profiles or their Fourier transforms by theoretical functions of size and strain broadening. The fitting procedure gives the median and the variance of the size distribution of crystallites, the density and the arrangement parameter of dislocations and one parameter for the edge or screw character of dislocations. Here it is noted that the median of the size distribution function is used only to parametrize the function itself, the crystallite or domain size is characterized by the mean values obtained from the median and the variance [7], see for example the volume-weighted mean value in Eq. (1) below. If there is evidence of shape anisotropy of crystallites from other type of investigations (e.g., transmission electron microscopy, TEM), the MWP method can also provide the aspect ratio of the crystallites [31].

In this paper, the microstructure of nanocrystalline Al–Mg alloys produced by ball milling of Al and Mg powders is investigated by X-ray diffraction peak profile analysis. The crystallite size distribution and the dislocation structure are determined and the hardness of the compacted powders is also measured as a function of the nominal Mg content and the milling time. It is shown that the two components are mechanically alloyed by ball milling beyond the equilibrium solubility limit at room temperature (RT) with a very fine microstructure.

2. Experimental

2.1. Sample preparation

A series of aluminum–magnesium samples were prepared from high purity aluminum (99.9%) powder and high purity magnesium chips (less than 2 mm thick and 5 mm long). The mechanical alloying was carried out using a Spex8000 shaker miller at room temperature. The charge was loaded into a steel vial in a glove box with a purified argon (<3 ppm oxygen) atmosphere. Martensitic stainless steel (440 °C) balls with diameters of 6.4 and 7.9 mm were used for milling with a ball-to-powder ratio of 10:1. Stearic acid (2%) was used as a control agent to prevent severe cold welding. Since both, the balls and the vial of the mill are made of hardened steel, the iron contamination in the soft Al alloy is very small, below 0.02 at.%. Aluminum with 6 wt.% magnesium alloys were milled for 0.5, 1, 3 and 6 h. A series of Al–x wt.% Mg (x = 0, 3, 6) were milled for 3 h at the same conditions to study the effect of the nominal Mg content. The milled powders were compacted at a pressure of 1 GPa in air at room temperature without any lubricant. The diameter of the pressure die was 6.35 mm and the powders were pressed for 5 min. The surface of the compacted specimens was polished carefully for hardness measurements.

2.2. Indentation measurements

The hardness was measured by depth-sensing indentation tests (DSIs) [32]. The DSI measurements were carried out by a Shimadzu-made dynamic ultra-micro hardness tester (DUH 202). Each DSI test consisted of a loading–unloading cycle. During the loading period a Vickers indenter penetrated into the surface of the sample at constant loading rate (2.65 mN/s) and the same rate was applied in the unloading period when the pyramid moved backwards. The maximum load in each test was 100 mN.

2.3. X-ray diffraction analysis

The microstructure of both the ball-milled powders and the compacted specimens were studied by X-ray diffraction peak profile analysis. The diffraction profiles were measured by a Philips X'pert powder diffractometer using Cu anode and pyrolithic graphite secondary monochromator. Step size and step time were 0.03° and 22 s per step, respectively. The X-ray diffraction profiles were evaluated for the crystallite size distribution and the dislocation structure by the multiple whole profile fitting procedure described in detail in [29,30]. In this method the Fourier transforms of the experimental profiles corrected for instrumental broadening are fitted by the product of the physically well established theoretical Fourier coefficients corresponding to size and strain profiles. In the calculation of the theoretical functions, the crystallites are modeled by spheres with log-normal size distribution and it is assumed that the strain is caused by dislocations. For dislocated crystals the theoretical Fourier transform of the strain profile was derived by Wilkens [17,18]. This Fourier transform, called Wilkens function, is used in the MWP fitting procedure for describing strain. The major steps of the method are:

1. The background subtraction and the separation of overlapping peaks are carried out as follows. Let us consider two overlapping peaks, no. 1 and no. 2. Auxiliary analytical functions (Voigt, pseudo-Voigt or PearsonVII) plus a linear background are fitted to the overlapping peaks. In the next step the background and the analytical function fitted to no. 1 are subtracted from the measured data. The data remaining after this subtraction are considered as the experimental data of the peak no. 2. In a further step, the same procedure is performed again with subtracting the background and the analytical function fitted to no. 2 from the original measured data. Now the data remaining after this second subtraction are considered as the experimental data of the individual peak no. 1. Here we note that the two peaks obtained by this procedure are still represented by the measured datapoints in spite that the subtraction of the overlapping peak is carried out by using the analytically fitted function. It is noted that the selection of a particular analytical function has an unavoidable effect, especially in the tail regions, on the shape of the profile obtained after separation.
2. The Fourier transform of the experimental data of individual profiles are determined by a non-equidistant sampling Fourier transformation and the experimental Fourier transforms are corrected for instrumental broadening by the Stokes method [33] using NIST SRM660a LaB_6 peak profile standard material. The sampling is non-equidistant since the measured data are equidistant in 2Θ, which are transformed before Fourier transformation into the variable $K = 2\sin\Theta/\lambda$, a non-linear function of 2Θ. Though the linear absorption of LaB_6 is larger than that of Al, due to the strong physical peak broadening of the investigated samples this difference has only a slight effect on the results of the instrumental corrections.
3. The corrected Fourier transforms are normalized and fitted simultaneously by the products of the theoretical size and strain Fourier transforms using the Marquardt–Levenberg least squares method [30].

The procedure is based on five fitting parameters in the case of cubic crystals: (i) the median (m), (ii) the variance (σ) of the log-normal size distribution function, (iii) the dislocation density (ρ), (iv) the dislocation arrangement parameter ($M = R_e\sqrt{\rho}$, where R_e is the effective outer cut-off radius of dislocations [17]) and (v) the parameter q describing the average dislocation contrast factors and the edge or screw character of dislocations. The value of M gives the strength of the dipole character of dislocations—the higher the value of M, the weaker the dipole character and the screening of the displacement fields of dislocations. From m and σ the arithmetic, the area- and the volume-weighted mean sizes (diameters) of the crystallites can be determined [7]. Here, we note that the numerical fitting procedure provides only the median, m, and the variance, σ, of the log-normal size distribution. From these two values, however, as mentioned before, any of the average size parameters weighted in different ways can be obtained. As it can be established from the values of m and σ given below, in the present case the trend in the changing of all these three mean-size values is the same with changing the milling time or the nominal Mg content. Therefore, in this paper only the volume-weighted mean crystallite size, $\langle x\rangle_{vol}$, is reported which correlates with the apparent size parameter, $d = 1/\beta$, where β is the integral breadth of the profiles. The volume-weighted mean crystallite size or diameter is calculated from m and σ as [7]:

$$\langle x\rangle_{vol} = m\exp(3.5\sigma^2). \quad (1)$$

3. Results and discussion

Fig. 1 shows the X-ray diffractogram of Al–6 wt.% Mg powder mixture ball-milled for 0.5 h in logarithmic intensity scale. As it can be seen from the figure the main phase is the Al–Mg solid solution. The reflections corresponding to this phase are indicated with their indices. At the same time the most intense Bragg peaks of Mg also appeared in the neighborhood of the first two reflections of Al–Mg. These peaks are clearly visible in Fig. 2a, where the part of Fig. 1 corresponding to the 2Θ region between 30 and 53° is replotted also in logarithmic intensity scale. After 6 h milling the peaks of Mg almost completely disappeared and the Al–Mg peaks were shifted to lower 2Θ values (see Fig. 2b) which corresponds to the dissolution of the larger Mg atoms into the Al matrix. The lattice constant of the Al–Mg alloys produced by mechanical alloying was obtained from the positions of the X-ray diffraction peaks. The Mg concentration in the solid solution was determined from the value of the lattice parameter using the Vegard's plot of Pool and Axon [34]. In Fig. 3, the small open circles show the lattice parameters of Al–Mg alloys for different Mg concentrations determined by Pool and Axon and the solid line is connecting these circles. The measured values of the lattice constants of the mechanically alloyed samples are placed on this

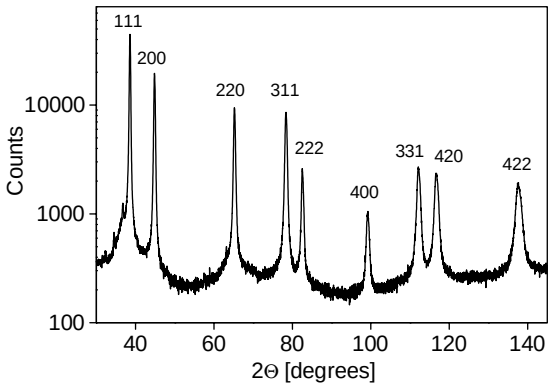

Fig. 1. The X-ray diffractogram of Al–6 wt.% Mg powder mixture milled for 0.5 h in logarithmic intensity scale. The peaks with the indices are the reflections corresponding to Al–Mg solid solution.

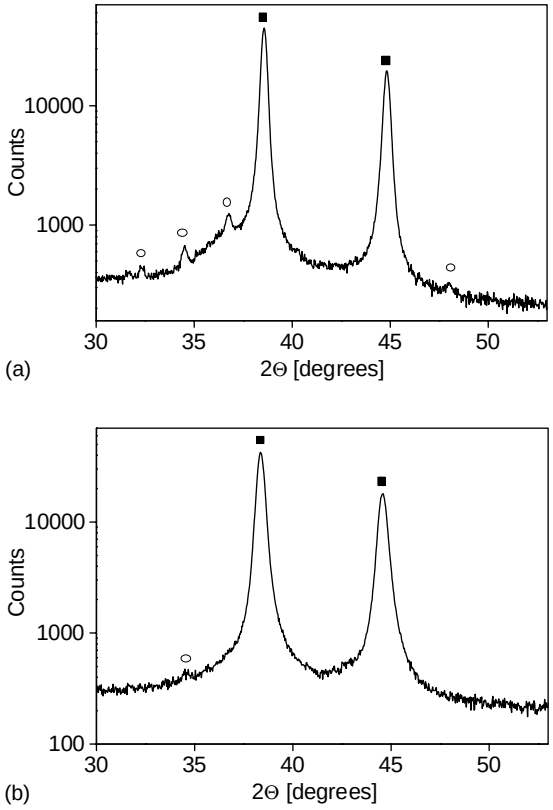

Fig. 2. The enlarged part of the X-ray diffractogram in the angular range $2\Theta = 30$ to 53°—(a) for the Al–6 wt.% Mg powder milled for 0.5 h and (b) for the same powder milled for 6 h. The solid squares and the open circles represent the peaks of Al–Mg solid solution and Mg, respectively.

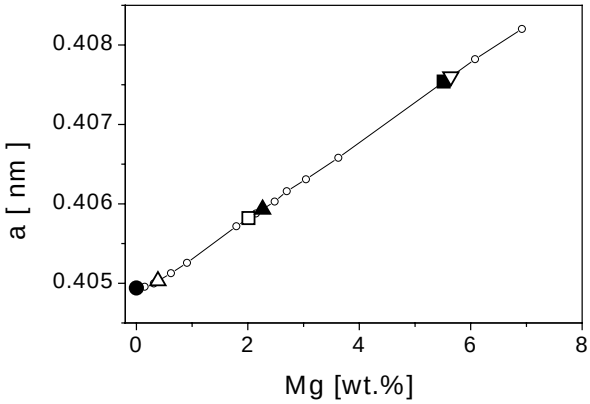

Fig. 3. The lattice constants vs. the Mg concentration in Al–Mg alloys. The small open circles represent the data measured by Pool and Axon [34] and the solid line connects these points. The Mg concentration in the mechanically alloyed samples were obtained by searching for the Mg contents corresponding to the measured lattice parameters (large symbols)—Al–6 wt.% Mg milled for 0.5 h (open up-triangle), 1 h (open square), 3 h (solid square), 6 h (open down-triangle) and the samples milled for 3 h with the nominal Mg content of 0 wt.% (solid circle), 3 wt.% (solid up-triangle) and 6 wt.% (solid square).

solid line. These values are represented by the large symbols in Fig. 3. The legend of the symbols is given in the figure caption. The Mg concentration in the solid solution of the mechanically alloyed samples is obtained as the abscissa coordinate corresponding to the large symbols. The lattice constants and the Mg concentrations in solid solution of Al–6 wt.% Mg powders milled for different time periods are listed in Table 1a. The same parameters of powders with different nominal Mg contents milled for 3 h are listed in Table 1b. As it can be seen from the tables, the Mg concentration in solid solution is increasing with the milling time for one particular powder composition and it is also increasing with the nominal Mg content for one particular milling time. After milling the powder containing nominally 6 wt.% Mg for 3 h, the Mg concentration in the solid solution reaches 5.52 wt.% and does not increase further significantly by 6 h milling (see Table 1a). This means that after milling for 3 h almost all of the Mg content (about 6 wt.%) goes into solid solution. The solubility limit of Mg in Al at 100 °C is 1.9 wt.% (2.1 at.%) [35–37]. At room temperature it is definitely below this value, as it can be seen from the phase diagram on page 106 in [38]. As it can be seen in Fig. 3 and Table 1a this value is well exceeded by mechanical alloying. This is in agreement with the nonequilibrium state of the alloys produced by high energy ball milling [39,40].

The measured and the fitted Fourier transforms are shown in Fig. 4a for the Al–6 wt.% Mg specimen after ball milling for 0.5 h. For the sake of a more detailed presentation of the quality of the fitting, the measured (open circles) and fitted (solid lines) Fourier transforms corresponding to the 331, 420 and 422 reflections are shown in a wider scale in Fig. 4b. The difference between the measured and the fitted values is also plotted in the lower parts of the figures with the same scaling as in the main parts of the figures. The quality of the fitting is characterized quantitatively by the weighted least-squares error (R_{wp}) [26] where the weights are the reciprocal of the observed Fourier transforms. (Here

Table 1a
The lattice parameter (a), the Mg concentration in solid solution and the microstructural parameters determined from X-ray diffraction for the powder mixture of the nominal composition Al–6 wt.% Mg milled for different periods

Milling time (h)	a (nm)	Mg (wt.%)	m (nm)	σ	$\langle x \rangle_{vol}$ (nm)	$\rho \times 10^{14}$ (m^{-2})	M	q	R_{wp} (%)
0.5	0.40503(4)	0.39(8)	28(3)	0.41(3)	50(7)	14(2)	2.0(2)	0.65(5)	2.5
1	0.40582(3)	2.01(6)	18(2)	0.37(3)	29(3)	72(6)	1.6(2)	0.40(4)	3.1
3	0.40754(4)	5.52(6)	19(2)	0.40(3)	33(3)	72(6)	1.0(2)	0.38(4)	4.6
6	0.40760(5)	5.64(8)	19(2)	0.38(3)	31(3)	83(7)	1.0(2)	0.47(5)	4.2

The weighted least-squares errors (R_{wp}) are also listed.

Table 1b
The lattice parameter (a), the Mg concentration in solid solution and the microstructural parameters determined from X-ray diffraction for the powders with different nominal Mg content milled for 3 h

Nominal Mg (wt.%)	a (nm)	Mg (wt.%)	m (nm)	σ	$\langle x \rangle_{vol}$ (nm)	$\rho \times 10^{14}$ (m^{-2})	M	q	R_{wp} (%)
0	0.40491(3)	0.00(7)	60(6)	0.18(2)	67(8)	19(2)	1.0(2)	0.72(5)	8.9
3	0.40593(5)	2.26(8)	33(3)	0.21(3)	39(4)	40(4)	1.2(2)	0.54(5)	2.4
6	0.40754(4)	5.52(6)	19(2)	0.40(3)	33(3)	72(6)	1.0(2)	0.38(4)	4.6

The weighted least-squares errors (R_{wp}) are also listed.

we note that, R_{wp} is only used to characterize the quality of the fit, whereas, no weighting of the Fourier coefficients was applied during the fitting procedure.) The measured diffraction patterns have been reconstructed by convoluting the instrumental pattern of LaB_6 with the inverse Fourier transform of the fitted theoretical Fourier coefficients and adding an appropriate polynomial function for the background. As an example, the measured and reconstructed patterns of the specimen ball milled for 6 h are shown in Fig. 5 in linear scale. In the inset the patterns are plotted in logarithmic intensity scale. Due to the small crystallite size and high density of crystal defects, especially dislocations, the quality of the diffraction patterns cannot be compared to patterns corresponding to well-annealed and defect-free powder samples. In spite of that, thanks to the extremely long measuring period and the well aligned diffractometer (see Section 2) the quality of the measured patterns is sufficient for evaluating the microstructural parameters. The relatively good fit shown by the plots indicates that the parameters determined by fitting the Fourier coefficients provide a satisfactory reproduction of the measured pattern. The microstructural parameters obtained from the fitting procedure and the values of R_{wp} are listed in Tables 1a and 1b. The volume-weighted crystallite size, the dislocation density and the Mg concentration as a function of the milling time and the nominal Mg content are plotted in Figs. 6 and 7, respectively. For the Al–6 wt.% Mg samples the Mg concentration increases with milling time up to 3 h. After 3 h there is no changes in the Mg concentration. The dislocation density increases while the crystallite size decreases rapidly with milling time up to 1 h. Between 1 and 6 h milling time the dislocation density and the crystallite size do not change significantly, as shown in Fig. 6. At the same time the value of the M parameter decreases with the milling time up to 3 h indicating that the dipole character of the dislocations increases. Between 3 and 6 h milling periods the M parameter does not change.

In the case where the nominal Mg content changes and the milling time period is fixed to 3 h, the Mg concentration in the solid solution and the dislocation density increase while the crystallite size decreases with increasing nominal Mg content, as shown in Fig. 7 and in Table 1b.

The character of dislocations can be obtained from the value of the q parameter. The q parameter values in

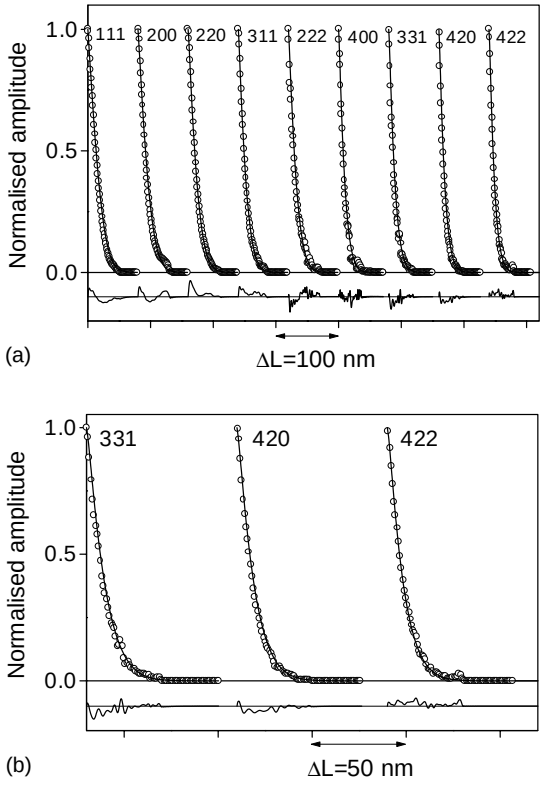

Fig. 4. The measured and the fitted Fourier transforms of the diffraction profiles of the Al–6 wt.% Mg powder milled for 0.5 h (a), three selected Fourier transforms are shown in a wider scale in (b). The difference between the measured and the fitted values is also plotted in the lower parts of the figures. The scaling of the differences is the same as in the main parts of the figures.

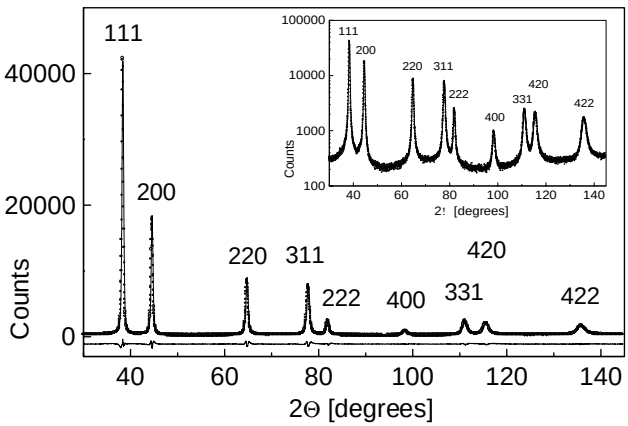

Fig. 5. The measured (open circles) and reconstructed (solid lines) patterns of the specimen ball milled for 6 h. In the inset the patterns are plotted in logarithmic intensity scale.

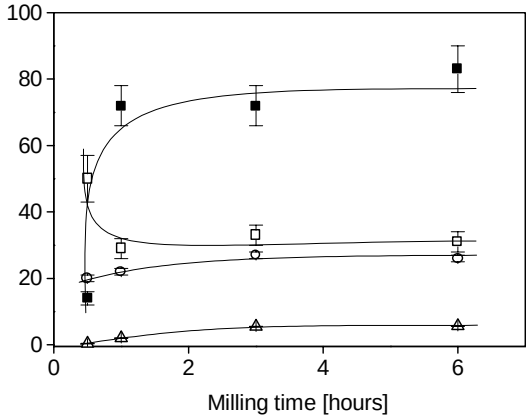

Fig. 6. The volume-weighted mean crystallite size in nanometers (open squares), the dislocation density in $10^{14}\,m^{-2}$ (solid squares), the Mg concentration in wt.% (open triangles) and the hardness in 10^{8} Pa (open circles) as a function of the milling period for the specimen of Al–6 wt.% Mg nominal composition.

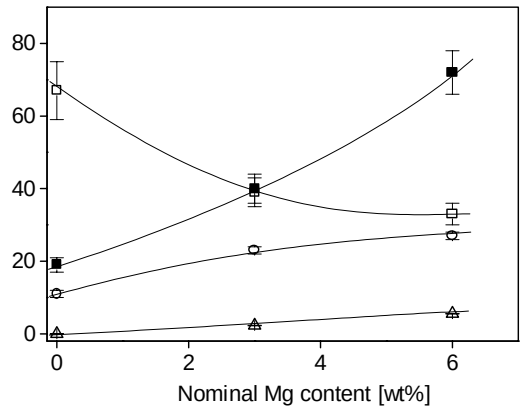

Fig. 7. The volume-weighted mean crystallite size in nanometers (open squares), the dislocation density in $10^{14}\,m^{-2}$ (solid squares), the Mg concentration in wt.% (open triangles) and the hardness in 10^{8} Pa (open circles) as a function of the nominal Mg content for the specimens milled for 3 h.

aluminum for pure screw and edge dislocations in the $\langle 1\,1\,0\rangle$ $\{1\,1\,1\}$ slip system can be determined by using the detailed numerical calculations and equations in [23] and the elastic constants in [41]. According to this, for pure screw or edge dislocations the values of q are 1.33 or 0.36, respectively. The experimental values of the q parameters obtained for the present ball milled alloys are listed in Tables 1a and 1b. For all the alloys studied in this paper, the value of q is lower than the arithmetic average of pure edge and screw cases, 0.85, which means that the character of dislocations is more edge type. The edge character of dislocations becomes stronger with increasing the milling time for one particular powder composition and also with increasing the nominal Mg content for one particular milling time.

The dislocation structure and its thermal stability in Al–Mg alloys has been extensively studied in a number of earlier papers [42–46]. Based on transmission electron microscopy, it was claimed that during cold rolling the dislocation structure in Al–Mg alloys, in a similar way as in pure Al, is rearranged for minimising its energy, calling these arrangements low-energy dislocation structures, LEDS [43,44]. The rearrangement of dislocations is, however, influenced by the strong interaction between solute Mg atoms and dislocations which is a large constraint on the dislocation mobility [43,44]. As it was shown above, up to 1 h ball milling the dislocation density increases while its character shifts toward edge type. Similar tendency is observed when the nominal Mg content increases in the samples milled for 3 h. These changes in the dislocation structure are most probably caused by the more effective pinning of edge than screw dislocations by solute Mg atoms. Mg atoms have a larger atomic radius than Al atoms therefore they are preferentially diffusing to the dilatation side of edge dislocations [47] leaving screw dislocations unpinned. Due to this effect screw dislocations are annihilated more easily during the milling procedure.

For hardness measurements the ball milled powders were compacted. To check the effect of compaction on the microstructure, the parameters of the crystallite size distribution and the dislocation structure of the compacted specimens were determined by X-ray diffraction peak profile analysis. The parameters of the microstructure and the values of the weighted least-square error (R_{wp}) are shown for Al–6 wt.% Mg samples with different milling time in Table 2a and for the specimens milled for 3 h with different nominal Mg content in Table 2b. Comparing the microstructural parameters obtained before (see Tables 1a and 1b) and after compaction it is concluded that this procedure has only slight effects on the microstructure of the ball milled specimens. This means that the hardness measured on the compacted samples characterizes also the mechanical properties of the milled Al–Mg alloys.

The hardness of the compacted samples was measured by depth-sensing Vickers indentation tests. The load was

Table 2a
The microstructural parameters, the weighted least-squares error (R_{wp}) and the hardness for the specimens compacted from the powder mixture of the nominal composition Al–6 wt.% Mg after ball milling for different time periods

Milling time (h)	m (nm)	σ	$\langle x\rangle_{vol}$ (nm)	$\rho \times 10^{14}$ (m^{-2})	M	q	R_{wp} (%)	H (GPa)
0.5	33(3)	0.44(4)	65(8)	18(2)	2.0(2)	0.69(5)	7.0	2.0(1)
1	26(3)	0.30(2)	36(4)	67(5)	1.9(3)	0.42(3)	8.6	2.2(1)
3	21(2)	0.37(3)	34(3)	66(5)	1.1(2)	0.39(4)	4.5	2.7(1)
6	17(2)	0.41(4)	31(3)	97(9)	1.0(2)	0.46(4)	4.8	2.6(1)

Table 2b
The microstructural parameters, the weighted least-squares error (R_{wp}) and the hardness for the samples compacted from the powders with different nominal Mg contents milled for 3 h

Nominal Mg (wt.%)	m (nm)	σ	$\langle x \rangle_{vol}$ (nm)	$\rho \times 10^{14}$ (m^{-2})	M	q	R_{wp} (%)	H (GPa)
0	72(6)	0.22(2)	85(9)	21(2)	1.0(2)	0.67(5)	9.5	1.1(1)
3	37(3)	0.29(3)	50(7)	41(3)	1.4(2)	0.62(5)	4.9	2.3(1)
6	21(2)	0.37(3)	34(3)	66(5)	1.1(2)	0.39(4)	4.5	2.7(1)

selected to be so small (100 mN) that the diagonals of indentation patterns (8–15 μm) were about one-tenth of the diameter of the compacted particles (100–200 μm) determined by optical microscopy. Here we note that the size of the particles is much larger than the size of the crystallites (coherently scattering domains) measured by X-ray diffraction. The hardness (H) was calculated from the maximum load (F_m) and the maximum penetration depth (h_m) of the indentation curves by the following equation [32]:

$$H = \frac{0.03784 \times F_m}{h_m^2}. \quad (2)$$

The hardness number, H, may differ slightly from the value that could be calculated by optical measurement of the indentation due to piling up of the material around the pattern [48]. The hardness was preferred to be determined from the indentation curves against the optical measurement of the pattern because of the higher accuracy of the penetration depth comparing to the indentation diagonal. The hardness values for the compacted specimens are listed in Tables 2a and 2b and plotted in Figs. 6 and 7. Each value is obtained as the average of 10 measurements. With increasing milling time, the hardness increases slightly up to 3 h owing to the increasing Mg concentration, the increase of the dislocation density and the decrease of crystallite size. Upon increasing milling time from 3 to 6 h the hardness does not change further, in line with no variation of the Mg concentration and the microstructure.

The hardness determined for pure Al milled for 3 h, H = 1.1 GPa, is close to the value of 1.27 GPa obtained for Al milled for 10 h by Rodriguez et al. [49]. One can establish that the hardness is increasing with the increase of the nominal Mg content of powder mixture for a particular milling time. The hardness increment is caused by the increase of the Mg concentration in solid solution and also by the increase of the dislocation density and even by the decrease of the crystallite size [42]. The effect of the crystallite size on the hardness of Al–3% Mg alloy was studied by Furukawa et al. [50]. They have found that the Hall–Petch equation relating the hardness to the crystallite size is valid for bulk Al–3% Mg samples produced by severe plastic deformation with the crystallite size (d) between 100 nm and 100 μm

$$\mathrm{HV} = H_0 + kd^{-1/2}, \quad (3)$$

where H_0 and k are appropriate constants. For Al–3% Mg alloys produced by equal channel angular pressing (ECAP) Furukawa et al. have obtained H_0 = 0.46 GPa and k = 0.35 GPa $\mu m^{1/2}$. For Al–3% Mg deformed by high pressure torsion straining (HPT) H_0 = 0.475 GPa and k = 0.41 GPa $\mu m^{1/2}$ have been found [50]. For the ball milled Al–3 wt.% Mg (3 h) sample HV = 2.03 and 2.31 GPa are calculated from Eq. (3) taking d = 50 nm (see Table 2b) and using the H_0 and k constants values obtained for ECA pressed and the torsion deformed specimens, respectively. These calculated values are close to the value, 2.3 GPa, measured by DSI.

4. Conclusions

Al–Mg alloys have been produced by ball milling the mixture of Al and Mg powders. It has been shown that alloying of Mg into the Al matrix and the formation of nanostructures occur simultaneously. The Mg content of the solid solution increases with milling period. After 3 h milling the Mg concentration exceeds the equilibrium solubility limit at room temperature by a factor of almost three. On the other hand, while the Mg content of the solid solution is increasing monotonously until the Mg reserve in the powder mixture enables this, the refinement of the microstructure saturates much earlier. It is found that the Mg concentration has a strong effect on the defect structure. With increasing nominal Mg content of the powder mixture or with increasing milling time, the dislocation density increases and the character of dislocations is shifted toward edge type. This is explained by the increase of the solute Mg concentration which increases the pinning effect of Mg atoms on edge dislocations thus hindering their annihilation. The hardness obtained for the mechanically alloyed Al–3 wt.% Mg specimen is in correlation with the Hall–Petch relationship determined for bulk samples investigated in the literature.

Acknowledgements

This work was supported by the Hungarian Scientific Research Fund, OTKA, Grant Nos. T031786, T034666 and T046990. J.G. is grateful for the financial support of Magyary Zoltán postdoctoral program of Foundation for Hungarian Higher Education and Research (AMFK).

References

[1] L. Lu, Y.F. Zhang, J. Alloys Compd. 290 (1999) 279.
[2] J.H. Ahn, Y.K. Paek, J. Mater. Sci. Lett. 18 (1999) 17.

[3] G.K. Williamson, W.H. Hall, Acta Metall. 1 (1953) 22.
[4] B.E. Warren, B.L. Averbach, J. Appl. Phys. 21 (1950) 595.
[5] B.E. Warren, Prog. Met. Phys. 8 (1959) 147.
[6] J.G.M. van Berkum, A.C. Vermuelen, R. Delhez, T.H. de Keijser, E.J. Mittemeijer, J. Appl. Cryst. 27 (1994) 345.
[7] J.I. Langford, D. Louer, P. Scardi, J. Appl. Cryst. 33 (2000) 964.
[8] C.E. Krill, R. Birringer, Philos. Mag. A 77 (1998) 621.
[9] M. Rand, J.I. Langford, J.S. Abell, Philos. Mag. B 68 (1993) 17.
[10] A.J.C. Wilson, X-ray Optics, Methuen, London, 1962.
[11] J. Gubicza, J. Szépvölgyi, I. Mohai, L. Zsoldos, T. Ungár, Mater. Sci. Eng. A 280 (2000) 263.
[12] J. Gubicza, J. Szépvölgyi, I. Mohai, G. Ribárik, T. Ungár, J. Mater. Sci. 35 (2000) 3711.
[13] G. Caglioti, A. Paoletti, F.P. Ricci, Nucl. Instrum. 3 (1958) 223.
[14] P. Suortti, The Rietveld method, in: R.A. Young (Ed.), IUCr Monographs on Crystallography, vol. 5, Oxford University Press, 1993, p. 167.
[15] A.L. Bail, in: E. Prince, J.K. Stalick (Eds.), Proc. Accuracy in Powder Diffraction II, NIST Spec. Publ. No. 846, Gaithersburg, MD, 1992, p. 142.
[16] M.A. Krivoglaz, Theory of X-ray and Thermal Neutron Scattering by Real Crystals, Plenum Press, New York, 1996.
[17] M. Wilkens, Phys. Status Solidi A 2 (1970) 359.
[18] M. Wilkens, in: J.A. Simmons, R. de Wit, R. Bullough (Eds.), Fundamental Aspects of Dislocation Theory, vol. II, Nat. Bur. Stand. (US) Spec. Publ. No. 317, Washington, DC, USA, 1970, p. 1195.
[19] P. Klimanek Jr., R. Kuzel, J. Appl. Cryst. 21 (1988) 59.
[20] T. Ungár, A. Borbély, Appl. Phys. Lett. 69 (1996) 3173.
[21] P. Scardi, M. Leoni, J. Appl. Cryst. 32 (1999) 671.
[22] R. Kuzel, P. Klimanek, J. Appl. Cryst. 21 (1988) 363.
[23] T. Ungár, I. Dragomir, Á. Révész, A. Borbély, J. Appl. Cryst. 32 (1999) 992.
[24] T. Ungár, G. Tichy, Phys. Status Solidi A 171 (1999) 425.
[25] I.C. Dragomir, T. Ungár, J. Appl. Cryst. 35 (2002) 556.
[26] D. Balzar, J. Res. Natl. Inst. Stand. Technol. 98 (1993) 321.
[27] P. Scardi, M. Leoni, Y.H. Dong, Eur. Phys. J. B 18 (2000) 23.
[28] P. Scardi, M. Leoni, Acta Cryst. A58 (2002) 190.
[29] T. Ungár, J. Gubicza, G. Ribárik, A. Borbély, J. Appl. Cryst. 34 (2001) 298.
[30] G. Ribárik, T. Ungár, J. Gubicza, J. Appl. Cryst. 34 (2001) 669.
[31] T. Ungár, J. Gubicza, G. Ribárik, C. Pantea, T.W. Zerda, Carbon 40 (2002) 929.
[32] J. Gubicza, A. Juhász, J. Lendvai, J. Mater. Res. 11 (1996) 2964.
[33] A.R. Stokes, Proc. Phys. Soc. London 61 (1948) 382.
[34] D.M. Pool, H.J. Axon, J. Inst. Met. 80 (1952) 599.
[35] K. Eickhoff, H. Vosskühler, Z. Metallkd. 44 (1953) 223.
[36] J.L. Murray, Bull. Alloy Phase Diagr. 3 (1982) 60.
[37] J. Balík, P. Lukác, L.P. Kubin, Scripta Mater. 42 (2000) 465.
[38] M. Hansen, K. Anderko, Constitution of binary alloys, in: R.F. Mehl, M.B. Bever (Eds.), Met. Met. Eng. Series, McGraw-Hill, New York, 1958, pp. 106–107.
[39] C. Suryanarayana, Prog. Mater. Sci. 46 (2001) 1.
[40] Á. Révész, J. Lendvai, T. Ungár, Mater. Sci. Forum 343–346 (2000) 326.
[41] R.F.S. Hearmon, in: K.H. Hellwege, A.,M., Hellwege (Eds.), Elastic Constant Data, Landolt-Bornstein: New Series, Springer, Berlin, 1979, pp. 1–39.
[42] M. Verdier, I. Groma, L. Flandin, J. Lendvai, Y. Bréchet, P. Guyot, Scripta Mater. 37 (1997) 449.
[43] D.A. Hughes, Acta Metall. 41 (1993) 1421.
[44] G.F. Dirras, M.-P. Biget, C. Rey, Scripta Mater. 33 (1995) 755.
[45] D. Kuhlmann-Wilsdorf, Mater. Sci. Eng. A 113 (1989) 1.
[46] B. Bay, N. Hansen, D.A. Hughes, D. Kuhlmann-Wilsdorf, Acta Metall. 40 (1992) 205.
[47] I. Kovács, J. Lendvai, E. Nagy, Acta Met. 20 (1972) 975.
[48] J. Gubicza, N. Rozlosnik, A. Juhász, J. Mater. Sci. Lett. 16 (1997) 1904.
[49] J.A. Rodriguez, J.M. Gallardo, E.J. Herrera, J. Mater. Sci. 32 (1997) 3535.
[50] M. Furukawa, Z. Horita, M. Nemoto, R.Z. Valiev, T.G. Langdon, Acta Mater. 44 (1996) 4619.